Available online at www.sciencedirect.com
SCIENCE DIRECT®
Journal of Solid State Chemistry 177 (2004) 745–751
JOURNAL OF SOLID STATE CHEMISTRY
http://elsevier.com/locate/jssc

Investigation of the quasi-ternary system $LaMnO_3$–$LaCoO_3$–"$LaCuO_3$"—I: the series $La(Mn_{0.5}Co_{0.5})_{1-x}Cu_xO_{3-\delta}$

F. Tietz,* A. Schmidt, and M. Zahid

Forschungszentrum Jülich GmbH, Institut für Werkstoffe und Verfahren der Energietechnik (IWV-1), D-52425 Jülich, Germany

Received 3 June 2003; received in revised form 1 August 2003; accepted 27 August 2003

Abstract

The $La(Mn_{0.5}Co_{0.5})_{1-x}Cu_xO_{3-\delta}$ series with $x = 0$, 0.05, 0.1, 0.2, 0.4, 0.6, 0.8 and 1 was synthesized by the Pechini method to obtain insight into the phase formation in the quasi-ternary $LaMnO_3$–$LaCoO_3$–"$LaCuO_3$" system caused by the instability of $LaCuO_3$ under ambient conditions. After sintering at 1100°C some remarkable results were obtained: $LaMn_{0.3}Co_{0.3}Cu_{0.4}O_{3-\delta}$ crystallized as a single phase in the orthorhombic perovskite structure typical of $LaCuO_3$. Among the synthesized compositions this compound showed the highest electrical conductivity in air at 800°C (155 S cm^{-1}) and also the highest thermal expansion coefficient ($\alpha_{30-800°C} = 15.4 \times 10^{-6}$ K^{-1}). The $LaCuO_{3-\delta}$ composition also crystallized as a single phase but in a monoclinic structure although previous investigations have shown that other phases are preferably formed after sintering at 1100°C. The electrical conductivity and thermal expansion coefficient were the lowest within the series of compositions, i.e. 9.4 S cm^{-1} and 11.9×10^{-6} K^{-1}, respectively.

Keywords: Perovskites; Electrical conductivity; Thermal expansion; Sintering behavior; $LaMnO_3$; $LaCoO_3$; $LaCuO_3$

1. Introduction

Perovskite-type oxides, especially $LaMeO_{3-\delta}$ with Me = Cr, Mn, Fe, Co, Ni, Cu, are of special interest due to their electrical and oxygen transport properties. It is well known that the chemical stability of these perovskites decreases as the atomic number increases from Cr to Cu [1,2]. At room temperature $LaCrO_3$ [3], $LaMnO_3$ [4] and $LaFeO_3$ [5] crystallize as orthorhombic perovskites, whereas $LaCoO_3$ [6], $LaNiO_{3-\delta}$ [7] and $LaCuO_{3-\delta}$ [8] have a rhombohedal perovskite structure. Additionally, for $LaCuO_{3-\delta}$ two different crystal structures have been reported: a rhombohedrally and a tetragonally distorted perovskite structure synthesized at higher and lower oxygen pressure, respectively [8,9]. The perovskite $LaCuO_{3-\delta}$ does not exhibit superconductive properties, because it is a metallic conductor over most of its stoichiometry range [8–10]. Furthermore, it is metastable in air at room temperature [11]. Under ambient conditions, however, the ternary oxides $La_2NiO_{4-\delta}$ and $La_2CuO_{4-\delta}$ with K_2NiF_4-type structure are more stable than the corresponding ABO_3 perovskites [1] and are formed during firing of the corresponding binary oxides.

The perovskites $LaMnO_3$, $LaCoO_3$ and some of their combinations have been widely investigated regarding their crystal structure, electrical and ionic conductivity, catalytic, magnetic and thermal expansion behavior [1,12–20]. The phase diagram of $LaMnO_3$–$LaCoO_3$ [21,22] shows a miscibility gap of the orthorhombic and rhombohedral perovskites at $0.28 < x < 0.5$ for the $LaCo_{1-x}Mn_xO_3$ system at 1100°C [22]. The phase diagrams of the La–Mn–Cu–O [23] and La–Co–Cu–O [24] systems were established for $T = 1100$°C and 1040°C, respectively. In the La–Mn–Cu–O system a solubility of copper in the orthorhombic perovskite $LaMn_{1-a}Cu_aO_3$ was found up to $a = 0.5$, whereas two oxide phases formed in the La–Co–Cu–O system: rhombohedral $LaCo_{1-b}Cu_bO_3$ and tetragonal $La_2Cu_{1-c}Co_cO_3$ with $0 < b < 0.3$ and $0 < c < 0.25$. A simultaneous investigation of the $LaMn_{1-a}Cu_aO_3$ and $LaCo_{1-b}Cu_bO_3$ series [25] has revealed that (a) up to $0 < a < 0.6$ or $b \leqslant 0.2$ a single rhombohedral perovskite was formed, respectively, (b) with $a = 0.8$ or $0.4 < b < 0.8$ additionally $La_2(Mn,Cu)O_{4-\delta}$ and CuO appeared and (c) with $a = b = 1$ only $La_2(Mn,Cu)O_{4-\delta}$ and CuO were found. The differences in observed crystalline phases

*Corresponding author. Fax: +49-2461-612-455.
E-mail address: f.tietz@fz-juelich.de (F. Tietz).

0022-4596/$ - see front matter © 2003 Elsevier Inc. All rights reserved.
doi:10.1016/j.jssc.2003.08.029

and the slightly different regions of the mentioned solid solutions indicate that experimental conditions may influence the phase boundaries of Cu-containing systems, especially when even more complex systems like La–Mn–Co–Cu–O are considered which has not been systematically investigated in detail yet.

In combination with $LaMnO_3$ and $LaCoO_3$, the $LaCuO_3$ is written here in quotation marks because it symbolizes one of the three apexes in the phase diagram but it crystallizes, in fact, as a mixture of $La_2CuO_{4-\delta}$ and CuO and will preferably lead to multiple-phase regions as in the $LaCo_{1-b}Cu_bO_3$ series. Therefore, the purpose of this work was to initiate a study on the quasi-ternary $LaMnO_3$–$LaCoO_3$–"$LaCuO_3$" system in air with respect to phase stability and determination of phase regions. In addition, the sintering behavior, electrical conductivity and thermal expansion were investigated as a function of the substitution of copper. As a first attempt, the $La(Mn_{0.5}Co_{0.5})_{1-x}Cu_xO_{3-\delta}$ series was chosen.

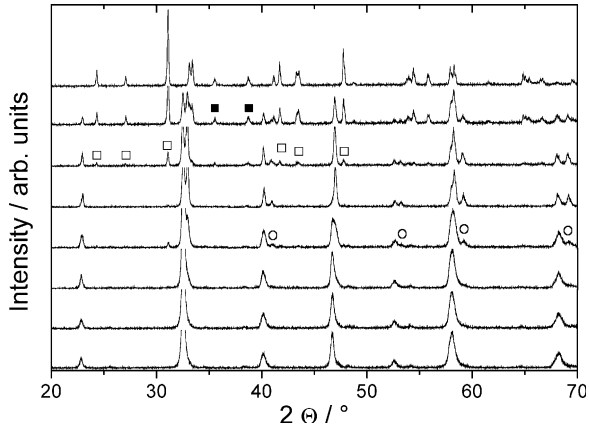

Fig. 1. XRD patterns of the $La(Mn_{0.5}Co_{0.5})_{1-x}Cu_xO_{3-\delta}$ series ($x = 0$, 0.05, 0.1, 0.2, 0.4, 0.6, 0.8, 1 from bottom to top) after heat treatment at 900°C for 6 h. The open circles and open squares indicate the formation of a rhombohedral perovskite (P_{rh}) and a K_2NiF_4-type phase, respectively. Starting from $x = 0.8$ also reflections of CuO (filled squares) appear in the upper XRD patterns.

2. Experimental

Eight powders with different compositions within the $La(Mn_{0.5}Co_{0.5})_{1-x}Cu_xO_{3-\delta}$ series ($x = 0$, 0.05, 0.1, 0.2, 0.4, 0.6, 0.8, 1) were synthesized by the Pechini method [26] using nitrate solutions of La, Mn, Co and Cu in the corresponding metallic ratios. A detailed description of the synthesis process is given in Ref. [27]. After obtaining the raw powder and calcination at 600°C for 3 h, the powders were characterized by differential thermal analysis and thermogravimetry (DTA/TG) up to 1400°C using a Netzsch STA 409. Additionally, two samples of each prepared powder were heat-treated at 900°C and 1100°C for 6 h. The crystal phase composition of these samples was determined by X-ray diffraction analysis using a Siemens D5000 diffractometer and CuK_α radiation.

The powders calcined at 600°C were uniaxially pressed to sticks ($40 \times 5 \times 4\,mm^3$) and, depending on the DTA results, sintered at 1100°C ($x \geqslant 0.4$) and 1300°C ($x \leqslant 0.3$) for 6 h. The total electrical conductivity of the sintered samples was measured by a 4-probe DC technique at temperatures between 100°C and 900°C in air using silver wires and silver paste as contacts. The thermal expansion between 30°C and 900°C as well as the sintering behavior as a function of temperature was determined using a Netzsch DIL 402C dilatometer.

3. Results and discussions

3.1. XRD and DTA/TG analysis

The XRD patterns of the samples heat-treated at 900°C are shown in Fig. 1. $LaMn_{0.5}Co_{0.5}O_{3-\delta}$ and $La(Mn_{0.5}Co_{0.5})_{0.95}Cu_{0.05}O_{3-\delta}$ crystallize as single-phase orthorhombic perovskites (P_{or}) with an XRD pattern similar to $LaCrO_3$ (space group *Pnma*, JCPDS file no. 33-701). With increasing copper content two additional phases are detected: a rhombohedral perovskite (P_{rh}), typical of the formation of $LaCuO_3$ (space group $R\bar{3}c$, JCPDS file no. 25-291), appears at $0.1 < x < 0.8$ and the $La_2CuO_{4-\delta}$-like compound (L2C) with K_2NiF_4-type crystal structure is obtained for $0.1 < x < 1$. The appearance of L2C should simultaneously lead to the formation of CuO, but it was not detected by XRD either because of the poor crystallinity of the minor phases, a sub-stoichiometry in lanthanum of the perovskites or even because of the small content below the resolution limit of XRD. However, a further increase in copper ($x \geqslant 0.6$) leads to the disappearance of P_{or} and to the appearance of CuO as a new phase besides P_{rh} and L2C. For $x = 1$, P_{rh} becomes unstable and only L2C and CuO are present.

A similar behavior can be observed in the samples calcined at 1100°C (see Fig. 2). The $La(Mn_{0.5}Co_{0.5})_{1-x}Cu_xO_{3-\delta}$ maintained an orthorhombic perovskite (P_{or}) structure for $x = 0$, 0.05 and 0.1. For $x = 0.2$ the P_{rh} can be detected as a second perovskite phase and at $x = 0.4$ only P_{rh} becomes the stable phase. A further increase in copper leads to the additional formation of L2C and CuO ($x = 0.6$ and 0.8). However, in contrast to the samples sintered at 900°C also $La_2Cu_2O_5$ (L2C2) with monoclinic crystal structure [28] appears. Finally, at the nominal composition $LaCuO_3$ ($x = 1$) only L2C2 is detected as a single phase. The detected crystalline phases formed under the investigated conditions are summarized in Table 1. The main differences in phase formation between the series sintered at 900°C and 1100°C start at $x = 0.4$ with the $LaCuO_3$-type perovskite being formed as a single

phase. This means that the cuprate structure can be stabilized under ambient conditions with the substitution of slightly larger cations. Additionally, the formation of $La_2Cu_2O_5$ instead of $La_2CuO_{4-\delta}$ is the second important difference between the two series. Because $La_2Cu_2O_5$ is formed without any remaining CuO, the reaction can be regarded as complete, whereas in cases where CuO could still be detected the phase formation did not seem to reach equilibrium. This also seems to be the case for the phases reported in Ref. [25]. It is surprising that this compound was obtained as a single phase, because it was reported previously that it could only be synthesized between 999°C and 1012°C [28]. This result and the phase formations reported previously [25,28] indicate that the stability regions with respect to temperature and composition for Cu-rich samples strongly depend on the precursors used, i.e. the synthesis route, the natural impurities of the starting materials as well as the impurities introduced during powder preparation (e.g. carbon). This might also lead to difficulties in establishing a reproducible phase diagram for the $LaMnO_3$–$LaCoO_3$–"$LaCuO_3$" system.

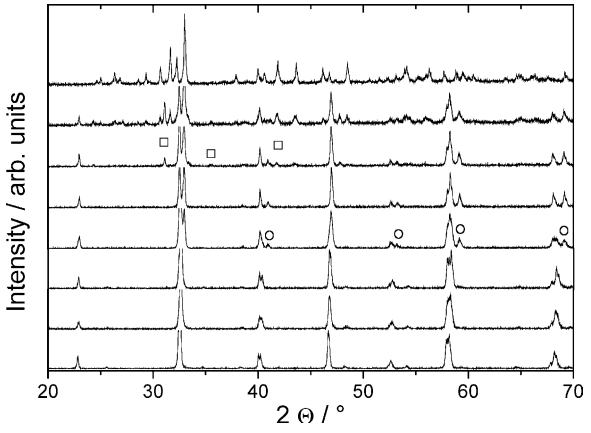

Fig. 2. XRD patterns of the $La(Mn_{0.5}Co_{0.5})_{1-x}Cu_xO_{3-\delta}$ series ($x = 0$, 0.05, 0.1, 0.2, 0.4, 0.6, 0.8, 1 from bottom to top) after heat treatment at 1100°C for 6 h. The open circles and open squares indicate the formation of a rhombohedral perovskite (P_{rh}) and a K_2NiF_4-type phase, respectively. Starting from $x = 0.8$ also reflections of $La_2Cu_2O_5$ appear in the upper XRD patterns.

The DTA measurements on the powders calcined at 600°C with $x \geqslant 0.4$ gave three endothermic peaks, two peaks between 1020°C and 1060°C and a third signal between 1320°C and 1360°C. The detailed temperature values are given in Table 2. According to the subsolidus relations for La_2O_3 and CuO [29] the first endothermic peak at 1022°C corresponds to the partial melting of the sample, where the solid phases $La_2Cu_2O_5$, $La_2CuO_{4-\delta}$ and CuO are in equilibrium with the melt (eutectic temperature), around 1050°C the CuO melts and the $La_2Cu_2O_5$ transforms to $La_2CuO_{4-\delta}$. At 1325–1356°C the samples decompose to La_2O_3 and liquid [29].

3.2. Dilatometry

The thermal expansion coefficients (TEC) were determined at temperatures between 30°C and 900°C in air. The thermal expansion curves are presented in Fig. 3a and show an increased slope with increasing Cu content up to $x = 0.4$. For $0 < x < 0.1$ the expansion curves exhibit a shape with a local minimum (Fig. 3b) indicating a phase transition. Because rhombohedral perovskites stabilize at elevated temperatures, it is assumed that the transition at 200°C for $LaMn_{0.5}Co_{0.5}O_{3-\delta}$ belongs to the orthorhombic–rhombohedral phase transition as also observed for $La_{1-x}Sr_xFe_{1-y}Co_yO_{3-\delta}$ perovskites [30]. At even higher temperatures, it is possible that the rhombohedral phase again transforms to an orthorhombic perovskite with $LaFeO_3$-type structure (JCPDS file no. 37-1493) [31]. The orthorhombic–rhombohedral phase transition decreases in temperature with increasing Cu content (150°C and 85°C for $x = 0.05$ and 0.1, respectively) and is suppressed below room temperature for $x \geqslant 0.2$. By increasing the Cu content towards $x = 1$ this leads to a decrease in thermal expansion. Fig. 4 shows the dependence of the TEC values between 30°C and 800°C on Cu content. At $x = 0.4$ a maximum value of $\alpha_{30-800°C} = 15.4 \times 10^{-6}\,K^{-1}$ is observed. In correlation with the XRD analyses of the samples sintered at 1100°C the observed increase in TEC up to $x = 0.4$ can

Table 1
Crystalline phases observed after sintering at 900°C and 1100°C

Nominal composition	Crystal structures of detected phases after calcination at 900°C for 6 h	Crystal structures of detected phases after calcination at 1100°C for 6 h
$LaMn_{0.5}Co_{0.5}O_{3-\delta}$	P_{or}	P_{or}
$LaMn_{0.475}Co_{0.475}Cu_{0.05}O_{3-\delta}$	P_{or}	P_{or}
$LaMn_{0.45}Co_{0.45}Cu_{0.1}O_{3-\delta}$	$P_{or} + P_{rh}$+L2C (+CuO[a])	P_{or}
$LaMn_{0.4}Co_{0.4}Cu_{0.2}O_{3-\delta}$	$P_{or} + P_{rh}$ + L2C (+CuO[a])	$P_{or} + P_{rh}$
$LaMn_{0.3}Co_{0.3}Cu_{0.4}O_{3-\delta}$	$P_{or} + P_{rh}$ + L2C (+CuO[a])	P_{rh}
$LaMn_{0.2}Co_{0.2}Cu_{0.6}O_{3-\delta}$	P_{rh}+L2C + CuO	P_{rh}+L2C + CuO
$LaMn_{0.1}Co_{0.1}Cu_{0.8}O_{3-\delta}$	P_{rh}+L2C + CuO	P_{rh}+L2C + L2C2 + CuO
$LaCuO_{3-\delta}$	L2C + CuO	L2C2

[a] Not detected by XRD.

Table 2
Endothermic DTA signals for $La(Mn_{0.5}Co_{0.5})_{1-x}Cu_xO_{3-\delta}$

Nominal composition	Temperature of Signal 1 (°C)	Temperature of Signal 2 (°C)	Temperature of Signal 3 (°C)
$LaMn_{0.5}Co_{0.5}O_{3-\delta}$	—	—	>1400
$LaMn_{0.475}Co_{0.475}Cu_{0.05}O_{3-\delta}$	—	—	>1400
$LaMn_{0.45}Co_{0.45}Cu_{0.1}O_{3-\delta}$	—	—	>1400
$LaMn_{0.4}Co_{0.4}Cu_{0.2}O_{3-\delta}$	—	—	>1400
$LaMn_{0.3}Co_{0.3}Cu_{0.4}O_{3-\delta}$	1024	1041	1331
$LaMn_{0.2}Co_{0.2}Cu_{0.6}O_{3-\delta}$	1021	1054	1356
$LaMn_{0.1}Co_{0.1}Cu_{0.8}O_{3-\delta}$	1023	1054	1349
$LaCuO_{3-\delta}$	1022	1050	1327

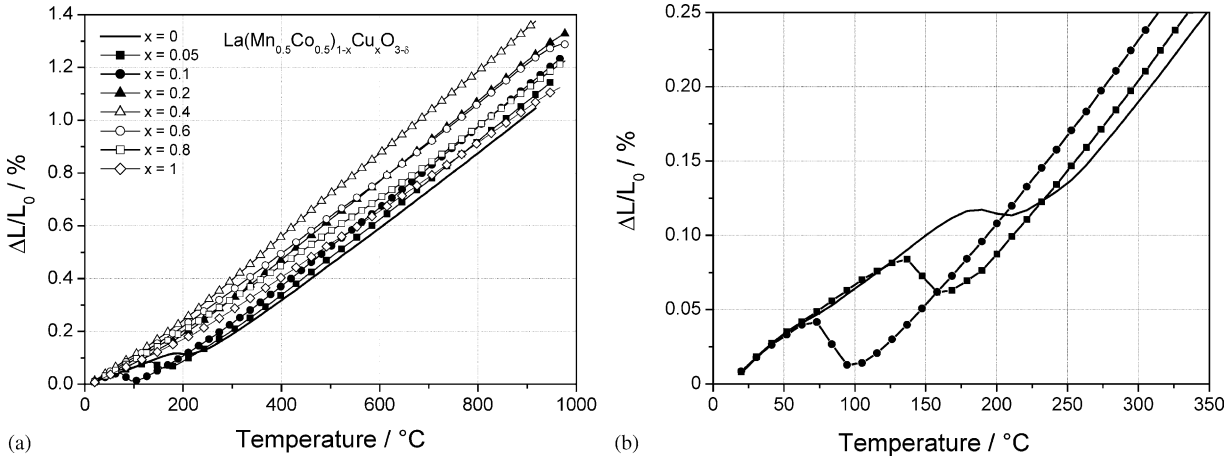

Fig. 3. (a) Thermal expansion curves for the $La(Mn_{0.5}Co_{0.5})_{1-x}Cu_xO_{3-\delta}$ series. (b) Enlarged low-temperature region of the expansion curves for $x = 0$, 0.05 and 0.1 (same symbols as in (a)).

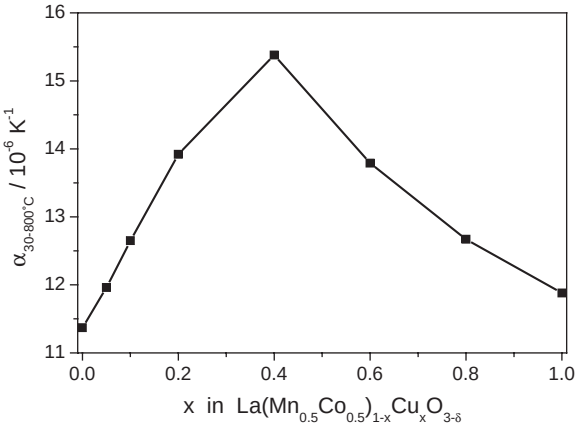

Fig. 4. Thermal expansion coefficients between 30°C and 800°C for the $La(Mn_{0.5}Co_{0.5})_{1-x}Cu_xO_{3-\delta}$ series.

be related to the formation of the P_{rh} phase, whereas the decrease in TEC for $x>0.4$ can be mainly attributed to the thermal expansion of L2C2 with $\alpha_{30-800°C} = 11.9\times 10^{-6}\,K^{-1}$.

The sintering behavior of the $La(Mn_{0.5}Co_{0.5})_{1-x}Cu_xO_{3-\delta}$ series was measured in a push-rod dilatometer using pressed pellets with a diameter of 8 mm and a thickness of 5 mm. A constant heating rate of $180\,K\,h^{-1}$ was applied up to 900°C and the samples were kept at maximum temperature for 5 h. Even at such a low sintering temperature considerable differences in the shrinkage of the samples are observed (Fig. 5). For a Cu content of up to $x = 0.1$ the linear shrinkage remains below 10% and is rather poor compared with the samples containing more copper. A more pronounced sintering occurs with $x>0.2$ and nearly 20% shrinkage is achieved with $LaMn_{0.3}Co_{0.3}Cu_{0.4}O_{3-\delta}$ and $LaMn_{0.2}Co_{0.2}Cu_{0.6}O_{3-\delta}$. For $x = 0.8$ the shrinkage is reduced to about 12% whereas the sample with $x = 1$ shows the highest shrinkage with nearly 30%. The discontinuity in the shrinkage values for $x = 0.8$ was first believed to result from different initial densities, but after determining the initial and final densities (Fig. 6) of the samples this does not seem to explain the lower sintering activity. Although the samples with $x\geqslant 0.4$ all have a density of more that $4\,g\,cm^{-3}$, the difference between final and initial density is the lowest for $x = 0.8$ and agrees with the dilatometric measurement in Fig. 5. In this case the initial density of $3.05\,g\,cm^{-3}$ is the

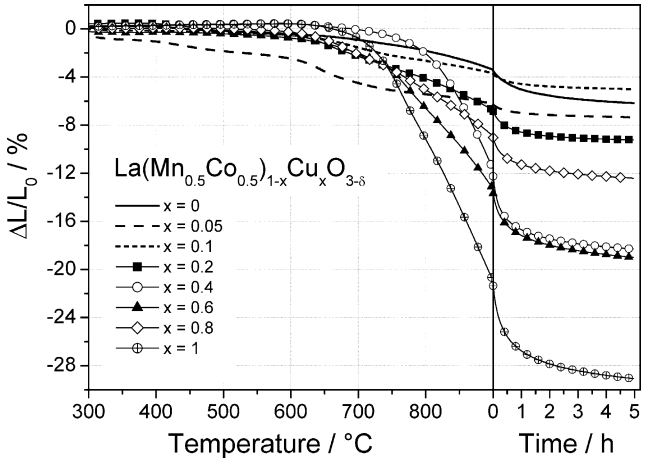

Fig. 5. Sintering curves between 300°C and 900°C and subsequent dwell time of 5 h at 900°C for the $La(Mn_{0.5}Co_{0.5})_{1-x}Cu_xO_{3-\delta}$ series.

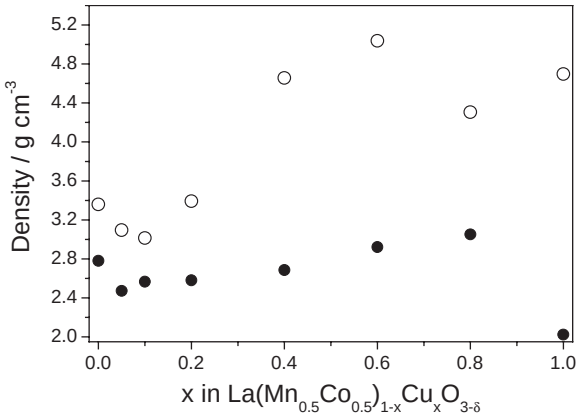

Fig. 6. Initial (●) and final (○) geometric densities of the samples used in the sintering experiments shown in Fig. 5.

highest for all samples, but it should not influence the densification curve to such an extent as shown in Fig. 5. The reason for the reduced sintering behavior might therefore be linked to the composition and phase formation at 900°C. Considering the phases present in the samples (Table 1), it seems that the CuO content has an influence on the sintering behavior. For $x = 0.6$ and 0.8 the sintering rate between about 650°C and 900°C is nearly constant, whereas the sintering rate for $x = 0.4$ (without CuO) is progressively increasing with temperature (Fig. 5). Therefore the CuO might act as a sintering inhibitor depending on its content (cf. Fig. 1) and the additional phases (P_{rh} + L2C for $x = 0.6$ and 0.8; only L2C for $x = 0.6$) in the samples.

3.3. Electrical conductivity measurements

Electrical conductivity of samples sintered at 1100°C and 1300°C for $x \geqslant 0.4$ and $x < 0.4$, respectively, was

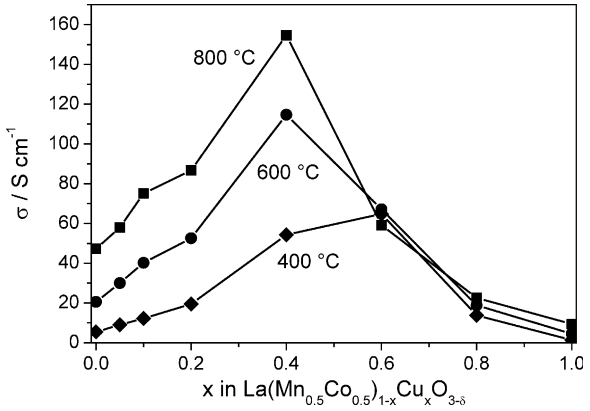

Fig. 7. Electrical conductivity at 400°C, 600°C and 800°C for the $La(Mn_{0.5}Co_{0.5})_{1-x}Cu_xO_{3-\delta}$ series.

measured between 100°C and 900°C in air. For all compositions a semiconductive temperature dependence was observed. At 600°C and higher temperatures a maximum electrical conductivity was found for $x = 0.4$, whereas for 400°C and lower temperatures this maximum shifted to $x = 0.6$ as shown in Fig. 7. The activation energies and the conductivity data measured at 800°C are listed in Table 3. It is apparent that the activation energy decreases when the conductivity is increased. However, the inverted proportionality is not strictly valid as the lowest activation energy was obtained at $x = 0.6$ and the highest conductivity was measured at $x = 0.4$, the composition at which P_{rh} appears as a single phase. Because $LaCuO_{3-\delta}$ shows a temperature-independent conductivity with 0.25 S cm^{-1} between −160°C and 60°C [8], it is interesting to note that the replacement of Mn and Co leads to a change in conductivity behavior from semi-metallic to semiconductive and to an increase in conductivity to 3.3 S cm^{-1} at 100°C. For a direct comparison, an extrapolation of the conductivity data in the Arrhenius plot (Fig. 8) yields 1.3 S cm^{-1} at 60°C.

As shown in Fig. 7, for $x \geqslant 0.6$ the conductivity decreases almost independently of the temperature reflecting, on the one hand, the low activation energy ($x = 0.6$) and, on the other hand, the low conductivities ($x = 0.8$, 1) of these samples. Since L2C2 was formed as a single phase at $x = 1$, the conductivity is shown explicitly in Fig. 8 together with two previous measurements carried out at low temperatures [28,32]. To our knowledge the data presented in Fig. 8 are the first high-temperature conductivity measurements reported for $La_2Cu_2O_5$.

4. Conclusions

This work was carried out to investigate the effect of the addition of copper on the physical properties of

Table 3
Electrical conductivity data for $La(Mn_{0.5}Co_{0.5})_{1-x}Cu_xO_{3-\delta}$

Nominal composition	Temperature range (°C)	Activation energy (eV)	$\sigma_{800°C}$ (S cm^{-1})
$LaMn_{0.5}Co_{0.5}O_{3-\delta}$	100–900	0.362±0.009	47.2
$LaMn_{0.475}Co_{0.475}Cu_{0.05}O_{3-\delta}$	100–900	0.338±0.006	58.0
$LaMn_{0.45}Co_{0.45}Cu_{0.1}O_{3-\delta}$	100–900	0.342±0.005	75.1
$LaMn_{0.4}Co_{0.4}Cu_{0.2}O_{3-\delta}$	300–900	0.303±0.003	86.7
$LaMn_{0.3}Co_{0.3}Cu_{0.4}O_{3-\delta}$	600–900	0.215±0.007	154.7
	100–500	0.248±0.007	
$LaMn_{0.2}Co_{0.2}Cu_{0.6}O_{3-\delta}$	500–900	0.042±0.005	59.2
	100–400	0.119±0.003	
$LaMn_{0.1}Co_{0.1}Cu_{0.8}O_{3-\delta}$	100–900	0.137±0.004	22.6
$LaCuO_{3-\delta}$	100–900	0.363±0.005	9.38

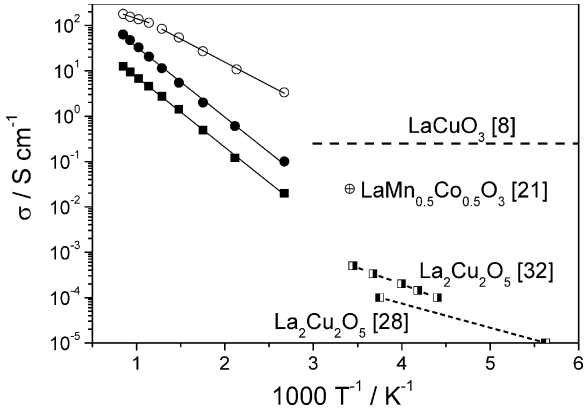

Fig. 8. Selected conductivity data from the $La(Mn_{0.5}Co_{0.5})_{1-x}Cu_xO_{3-\delta}$ series: (●) $x=0$ (pure P_{or}), (○) $x=0.4$ (pure P_{rh}) and (■) $x=1$ (pure L2C2). The straight lines correspond to the temperature regions considered for the determination of the activation energy in a σT vs. $1/T$ plot as listed in Table 3. For comparison with P_{or} and P_{rh}, one conductivity value at room temperature for $LaMn_{0.5}Co_{0.5}O_3$ (⊕ [21]) and the values for $LaCuO_3$ (– – – [8]) are inserted, respectively. Two measurements on L2C2 [28,32] in the low-temperature region are also included as dotted lines with half-filled squares.

oxides within the $LaMnO_3$–$LaCoO_3$–"$LaCuO_3$" quasi-ternary system. The addition of copper in this system leads to the formation of various phase mixtures depending on the amount of copper and the sintering temperatures. The $LaCuO_3$-perovskite structure, previously reported as a metastable phase, was detected as a stable, single-phase material for the composition $LaMn_{0.3}Co_{0.3}Cu_{0.4}O_{3-\delta}$. Additionally, the nominal composition $LaCuO_{3-\delta}$ crystallized as a $La_2CuO_{4-\delta}$ and CuO mixture and as pure $La_2Cu_2O_5$ after sintering at 900°C and 1100°C, respectively.

It was also the composition $LaMn_{0.3}Co_{0.3}Cu_{0.4}O_{3-\delta}$ that showed the highest electrical conductivity and thermal expansion. In addition, the sintering activity was strongly increased starting from this copper content. The changes in physical properties were related to the phases formed after sintering at 1100°C.

Acknowledgments

Financial support from the German Federal Ministry of Economics and Technology (BMWi) under contract O327088C/8-1.A is gratefully acknowledged.

References

[1] V.V. Kharton, A.A. Yaremchenko, E.N. Naumovich, J. Solid State Electrochem. 3 (1999) 303–326 (and references cited therein).
[2] H.U. Anderson, Solid State Ionics 52 (1992) 33–41.
[3] C.P. Khattak, D.E. Cox, Mater. Res. Bull. 12 (1977) 463–471.
[4] T. Hashimoto, N. Ishizawa, N. Mizutani, M. Kato, J. Crystal Growth 84 (1987) 207–211.
[5] S. Geller, E.A. Wood, Acta Crystallogr. 9 (1956) 563–568.
[6] A.N. Petrov, O.F. Kononchuk, A.V. Andreev, V.A. Cherepanov, P. Kofstad, Solid State Ionics 80 (1995) 189–199.
[7] J.L. García Muñoz, J. Rodríguez Carvajal, P. Lacorre, J.B. Torrance, Phys. Rev. B 46 (1992) 4414–4425.
[8] G. Demazeau, C. Parent, M. Pouchard, P. Hagenmuller, Mater. Res. Bull. 7 (1973) 913–920.
[9] J.F. Bringley, B.A. Scott, S.J. La Placa, T.R. McGuire, F. Mehran, Phys. Rev. B 47 (1993) 15269–15275.
[10] S. Darracq, S. Matar, G. Demazeau, Solid State Commun. 85 (1993) 961–965.
[11] I. Kaus, H.U. Anderson, Solid State Ionics 129 (2000) 189–200.
[12] V. Narasimhan, H.V. Keer, D.K. Chakrabarty, Phys. Stat. Sol. (a) 89 (1985) 65–71.
[13] R.A. De Souza, J.A. Kilner, Solid State Ionics 106 (1998) 175–187.
[14] T. Seiyama, Catal. Rev. Sci. Eng. 34 (1992) 281–300.
[15] S. Banerjee, V.R. Choudhary, Proc. Indian Acad. Sci. (Chem. Sci.) 112 (2000) 535–542.
[16] R. von Helmholt, J. Wecker, B. Holzapfel, L. Schultz, K. Samwer, Phys. Rev. Lett. 71 (1993) 2331–2333.
[17] A. Urushibara, Y. Moritomo, T. Arima, A. Asamitsu, G. Kido, Y. Tokura, Phys. Rev. B 51 (1995) 14103–14109.
[18] R.J. Radwański, Z. Ropka, Physica B 281&282 (2000) 507–509.
[19] F. Tietz, in: P. Vincenzini (Ed.), Proceedings of the Ninth CIMTEC-World Ceramic Congress and Forum on New Materials, Vol. 24, Techna Publishers S.r.l., Faenza, Italy, 1999, pp. 61–70.
[20] A. Petric, P. Huang, F. Tietz, Solid State Ionics 135 (2000) 719–728.
[21] G.H. Jonker, J. Appl. Phys. 37 (1966) 1424–1430.

[22] V.A. Cherepanov, E.A. Filonova, V.I. Voronin, I.F. Berger, J. Solid State Chem. 153 (2000) 205–211.
[23] I.L. Tikhonova, A.Yu. Zuev, A.N. Petrov, Russ. J. Phys. Chem. 72 (1998) 1625–1628.
[24] I.L. Tikhonova, A.V. Bakhtin, A.Yu. Zuev, A.N. Petrov, Russ. J. Phys. Chem. 73 (1999) 365–368.
[25] P. Porta, S. De Rossi, M. Faticanti, G. Minelli, I. Pettiti, L. Lisi, M. Turco, J. Solid State Chem. 146 (1999) 291–304.
[26] M.P. Pechini, US patent No. 3,330,697 (1967).
[27] F. Tietz, I. Arul Raj, W. Jungen, D. Stöver, Acta Mater. 49 (2001) 803–811.
[28] R.J. Cava, T. Siegrist, B. Hessen, J.J. Krajewski, W.F. Peck Jr., B. Batlogg, H. Takagi, J.V. Waszczak, L.F. Schneemeyer, H.W. Zandbergen, J. Solid State Chem. 94 (1991) 170–184.
[29] J.M.S. Skakle, A.R. West, J. Am. Ceram. Soc. 77 (1994) 2199–2202.
[30] L.-W. Tai, M.M. Nasrallah, H.U. Anderson, D.M. Sparlin, S.R. Sehlin, Solid State Ionics 76 (1995) 259–271, 273–283.
[31] R. Horyń, A. Sikora, E. Bukowska, J. Alloys Compd. 353 (2003) 153–169.
[32] T. Watanabe, C. Sekar, H. Shibata, A. Matsuda, Y. Zenitani, J. Akimitsu, Physica C 357–360 (2001) 380–383.